# Planetary Impacts

CHAPTER 43


Richard A.F. Grieve
Natural Resources Canada
Ottawa, Canada

Mark J. Cintala*
NASA Johnson Space Center
Houston, Texas

Roald Tagle
Humboldt University
Berlin, Germany




Planetary impacts have occurred throughout the history of the solar system. Small bodies, such as asteroids and comets, can have their orbits disturbed by gravitational forces, which results in their having a finite probability of colliding with another body or planet. Indeed, the collision of small bodies to form larger bodies was the fundamental process of planetary formation which, in its final stages, involved impacts between planetesimal-sized objects. As the solar system stabilized, the impact rate decreased but was still sufficient as late as ~4.0 billion years ago to produce impact basins with diameters measured in hundreds to thousands of kilometers. As a result, impacts were a major geologic process in early planetary evolution and served to characterize the early upper crusts and surfaces of planetary bodies. Although impacts producing craters 100–200 km in diameter are relatively rare in more recent geologic time, they still occur on timescales of approximately 100 million years. One such event on the Earth marks the boundary between the Cretaceous and Tertiary geologic periods and resulted in the mass extinction of approximately 75% of the species living on Earth 65 million years ago. The 180 km diameter Chicxulub impact crater in the Yucatan, Mexico, is now known to be the site of this global-extinction impact.

## 1. Impact Craters

### 1.1 Crater Shape

On bodies that have no atmosphere, such as the Moon, even the smallest pieces of interplanetary material can produce impact craters down to micrometer-sized cavities on individual mineral grains. On larger bodies, atmosphere-induced breakup and deceleration serve to slow smaller impacting objects. On the Earth, for example, impacting bodies with masses below $10^4$g can lose up to 90% of their velocity during atmospheric penetration, and the resultant impact pit is only slightly larger than the projectile itself. Atmospheric effects on larger masses, however, are less severe, and the body impacts with relatively undiminished velocity, producing a crater that is considerably larger than the impacting body.

The processes accompanying such events are rooted in the physics of impact, with the differences in response among the various planets largely being due to differences in the properties of the planetary bodies (e.g., surface gravity, atmospheric density, and target composition and strength). The basic shape of virtually all impact craters is

* The views expressed by the author are his own and do not represent the views of NASA or any NASA employee.

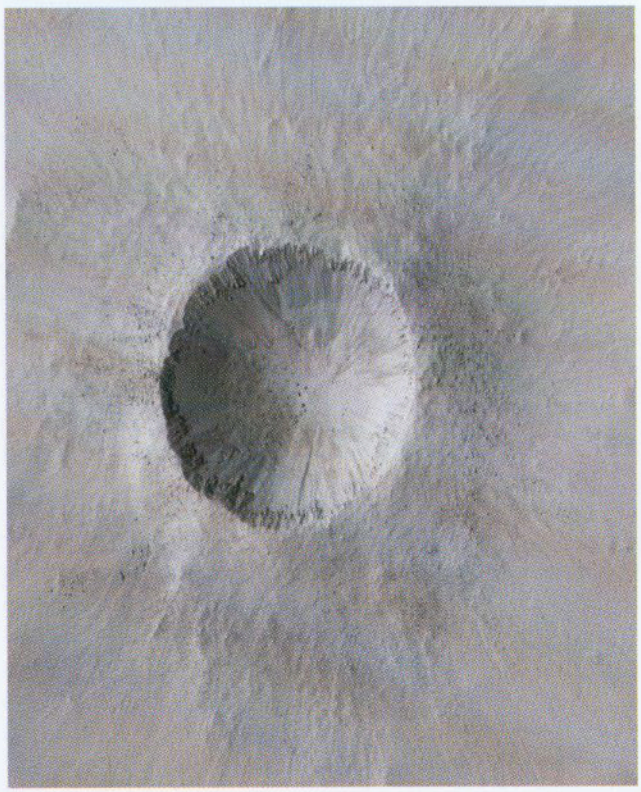

**FIGURE 1** Approximately 1 km diameter, relatively young simple martian crater. Large blocks, ejected late in the cratering process, can be seen on the ejecta near the rim. The ejecta can be differentiated into continuous ejecta and discontinuous ejecta, which appear as separate fingers and braids (*Mars Global Surveyor*).

a depression with an upraised rim. With increasing diameter, impact craters become proportionately shallower and develop more complicated rims and floors, including the appearance of central topographic peaks and interior rings.

There are three major subdivisions in shape: simple craters, complex craters, and impact basins Simple impact structures have the form of a bowl-shaped depression with an upraised rim (Fig. 1). An overturned flap of ejected target materials exists on the rim, and the exposed rim, walls, and floor define the apparent crater. Observations at terrestrial impact craters reveal that a lens of brecciated target material, roughly parabolic in cross section, exists beneath the floor of this apparent crater (Fig. 2). This breccia lens is a mixture of different target materials, with fractured blocks set in a finer-grained matrix. These are **allochthonous** materials, having been moved into their present position by the cratering process. Beneath the breccia lens, relatively in-place, or **parautochthonous**, fractured target materials define the walls and floor of what is known as the true crater (Fig. 2). In the case of terrestrial simple craters, the depth to the base of the breccia lens (i.e., the base of the true crater) is roughly twice the depth to the top of the breccia lens (i.e., the floor of the apparent crater).

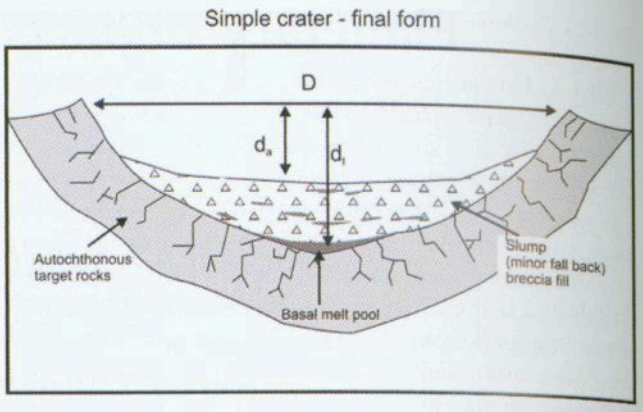


**FIGURE 2** Schematic cross section of a simple crater, based on terrestrial observations. $D$ is diameter and $d_a$ and $d_t$ are the depths of the apparent and true crater, respectively. See text for details.

With increasing diameter, simple craters display signs of wall and rim collapse, as they evolve into complex craters. The diameter at which this transition takes place varies between planetary bodies and is, to a first approximation, an inverse function of planetary gravity. Other variables, such as target strength, and possibly projectile type, and impact angle and velocity, play a role and the transition actually occurs over a small range in diameter. For example, the transition between simple and complex craters occurs in the 15–25 km diameter range on the Moon. The effect of target strength is most readily apparent on Earth, where complex craters can occur at diameters as small as 2 km in sedimentary target rocks, but do not occur until diameters of 4 km, or greater, in stronger, crystalline target rocks.

Complex craters are highly modified structures. A typical complex crater is characterized by a central topographic peak or peaks, a broad, flat floor, and a terraced, inwardly slumped rim area (Fig. 3). Observations at terrestrial complex craters show that the flat floor consists of a sheet of **impact melt** rock and/or **polymict** breccia (Fig. 4). The central region is structurally complex and, in large part, occupied by the central peak, which is the topographic manifestation of a much broader and extensive volume of uplifted rocks that occur beneath the center of complex craters (Fig. 4).

With increasing diameter, a fragmentary ring of interior peaks appears, marking the beginning of the morphologic transition from craters to basins. While a single interior ring is required to define a basin, they can be subdivided further into central-peak basins, with both a peak and ring; peak ring basins (Fig. 5), with a single ring; and multiring basins, with two or more interior rings (Fig. 6). The transition from central-peak basins to peak-ring basins to multiring basins also represents a sequence with increasing diameter. As with the simple to complex crater transition, there is a small amount of overlap in basin shape near transition diameters.

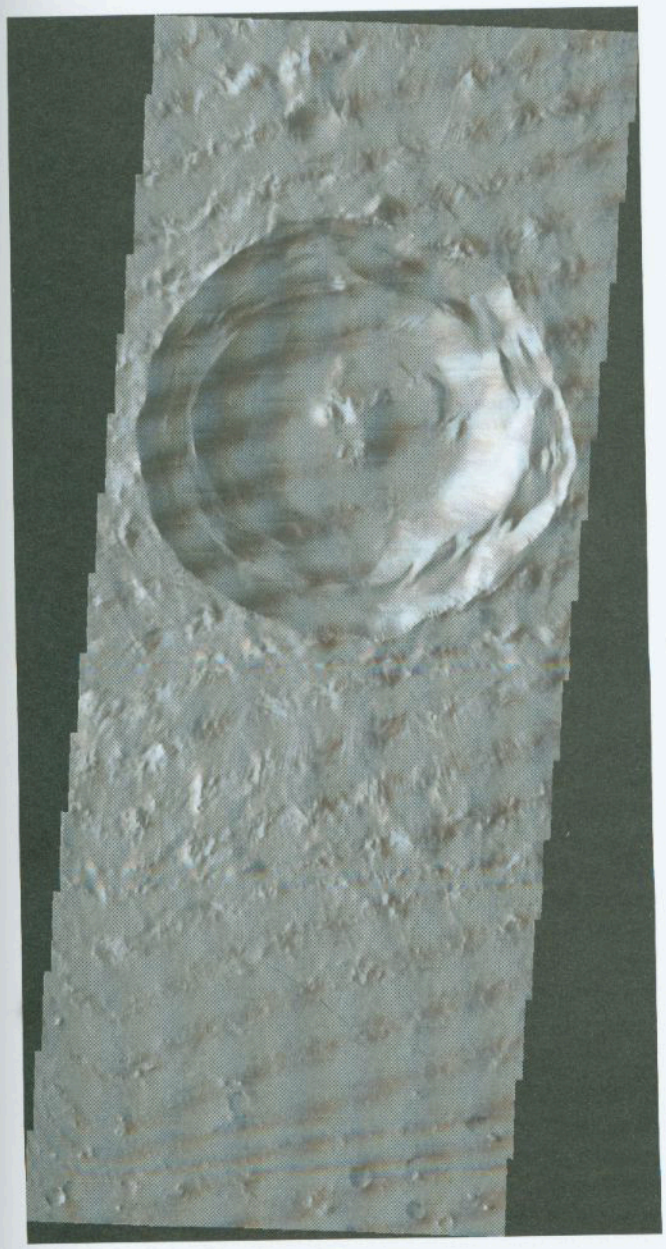

**FIGURE 3** Complex central peak crater in the Isidis basin on Mars, with the terraced walls of the crater rim stepping down to a flat floor and a central peak. Also evident are the external rays of continuous (linear) and discontinuous (braided) ejecta on the surrounding terrain. (*Mars Global Surveyor*).

Ejected target material surrounds impact craters and can be subdivided into continuous and discontinuous ejecta facies (Figs. 1 and 3). The continuous deposits are those closest to the crater, being thickest at the rim crest. In the case of simple craters, the net effect of the ejection process is to invert the stratigraphy at the rim. As the distance from the crater rim increases, the ejecta are emplaced at higher velocities and, therefore, land with higher kinetic energies, resulting in the mixing of ejecta with local surface material.

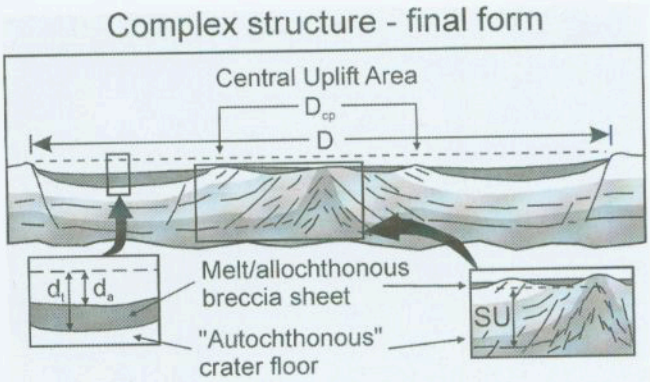


**FIGURE 4** Schematic cross section of a complex crater, based on terrestrial observations. Notation is as in Fig. 2, with SU corresponding to the structural uplift and $D_{cp}$, to the diameter of the central uplift area. Note the preservation of the upper beds (different shades of gray) in the outer portion of the crater floor, indicating excavation was limited to the central area. See text for details.

Thus, at increasing distance from the crater, the final ejecta blanket on the ground includes increasing amounts of local materials. Secondary crater fields, resulting from the impact of larger, coherent blocks and clods of ejecta, surround fresh craters and are particularly evident on bodies with no or thin atmospheres, such as the Moon, Mercury, and Mars. They are often associated with typically bright

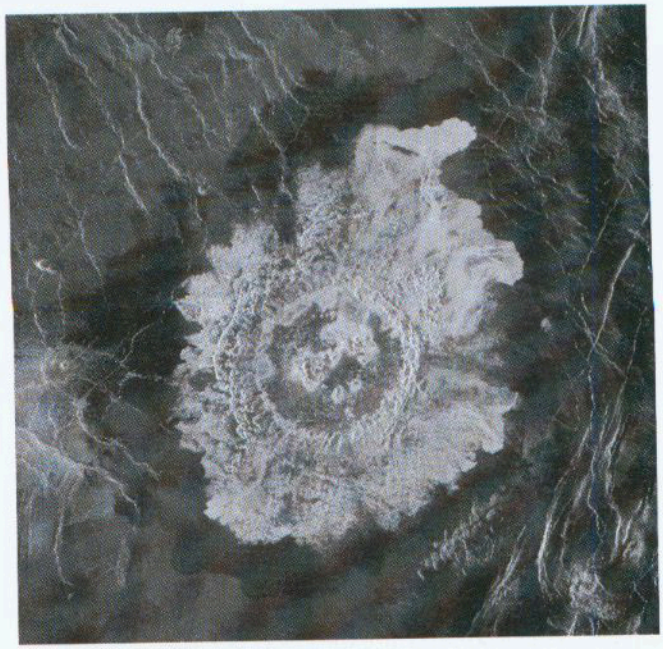

**FIGURE 5** The 50 km diameter peak ring basin Barton on Venus, with a discontinuous peak ring. Barton is close to the lower limit of the diameter where peak rings appear in impact craters on Venus and has a discontinuous peak ring (*Magellan*).

**FIGURE 6** With a diameter of ~900 km in diameter, as defined by the outer ring, the Cordillera mountains, Orientale the youngest and best-preserved multiring basin on the Moon (*Lunar Orbiter*).


**FIGURE 7** This 7.5 km diameter martian central peak crater is close to the transition diameter to complex craters and has a small central peak and simple terraced walls. Ejecta can be discriminated into a fluidized material, which extends farthest and has lobate margins, overlain by a second type of ejecta, which does not extend as far and displays radial linear features (*Mars Global Surveyor*).

or high-albedo "rays" that define an overall radial pattern to the primary crater. Two principal processes have been suggested to explain the rays. The first is a compositional effect, where the ejecta are chemically different from the material on which it is deposited. While this most often results in rays that are brighter than the surrounding material, the reverse can also occur. The second effect is a consequence of "maturity" due to prolonged exposure to "space weathering" agents like radiation and micrometeoroid bombardment on surface materials. [*See* MAIN-BELT ASTEROIDS.] Fresher material excavated by an impact and deposited in the rays is generally brighter than the more mature material of the deposition surface.

Many martian craters display examples of apparently fluidized ejecta (Fig. 7). They have been called "fluidized–ejecta," "rampart," or "pedestal" craters, where their ejecta deposits indicate emplacement as a ground-hugging flow. Most hypotheses on the origin of these features invoke the presence of ground ice (or water), which, upon heating by impact, is incorporated into the ejecta in either liquid or vapor form. This, then, provides lubrication for the mobilized material.

On Venus, impact craters more than 15–20 km in diameter exhibit central peaks and/or peak rings (Fig. 8) and appear, for the most part, to be similar to complex craters and basins on the other terrestrial planets. Many of the craters smaller than 15 km, however, have rugged, multiple floors or occur as crater clusters. This is attributed to the effects of the dense atmosphere of Venus (surface pressure of ~90 bar), which effectively crushes and breaks up smaller impacting bodies, so that they result in clusters of relatively shallow craters. Also due to atmospheric effects, there is a deficit in the number of expected craters with diameters up to 35 km, and there are no craters smaller than 3 km in diameter on Venus.

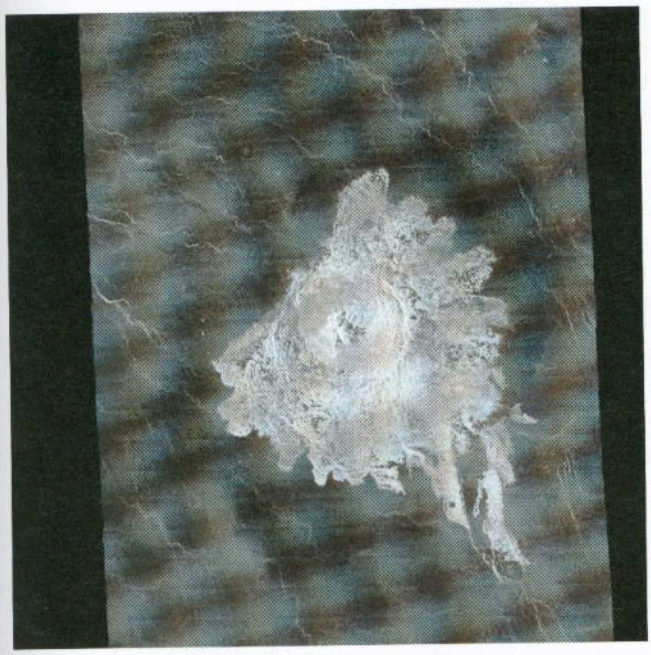

**FIGURE 8** Complex venusian central peak crater Aurelia, 32 km in diameter, which exhibits terraced walls, a flat floor, central peaks and long-running lobate flows, particularly in the lower right. Its ejecta pattern is asymmetric, indicating an oblique impact. The crater and the ejecta are also partially surrounded by terrain with a radar dark halo (*Magellan*).

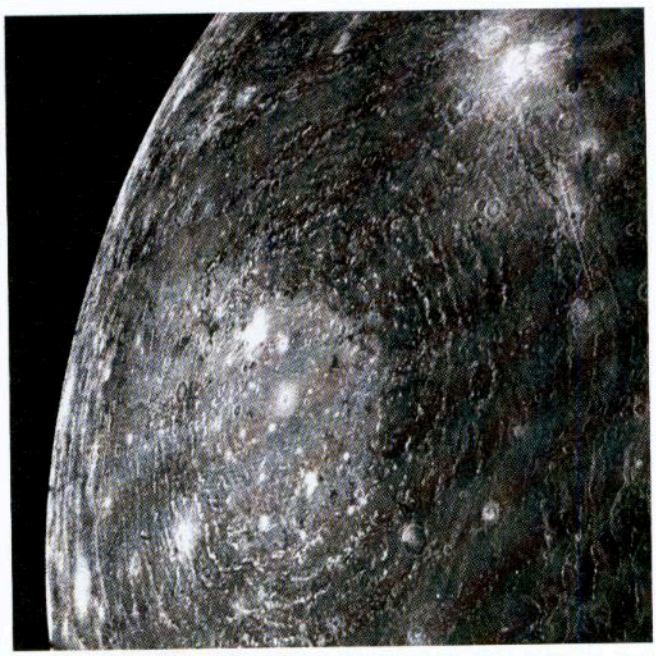

**FIGURE 9** The Valhalla multiring basin on Callisto. The overall structure may be as large as 4000 km in diameter, but only the central bright area is believed to be formed directly by impact. The surrounding, multiple scarps were likely formed in response to the subsurface flow of material back toward the initial crater, due to the relatively low internal strength of Callisto (*Voyager*).

In many cases, craters on Venus have ejecta deposits that are visible out to greater distances than expected from simple ballistic emplacement, and the distal deposits are clearly lobate (Fig. 8). These deposits likely owe their origin to entrainment effects of the dense atmosphere and/or the high proportion of impact melt that would be produced on a relatively high-gravity, high–surface temperature planet such as Venus. Another unusual feature on Venus is radar-dark zones surrounding some craters that can extend three to four crater diameters from the crater center (Fig. 8). They are believed to be due to the modification of surface roughness by the atmospheric **shock wave** produced by the impacting body. Small crater clusters have dark halos and dark circular areas where no central crater form has been observed. In these latter cases, the impacting body did not survive atmospheric passage, but the accompanying atmospheric shock wave had sufficient energy to interact with the surface to create a dark, radar-smooth area. [*See* VENUS: SURFACE AND INTERIOR.] The situation is somewhat analogous to the 1908 Tunguska event, when a relatively small body exploded over Siberia at an altitude of ~10 km, and the resultant atmospheric pressure wave leveled some 2000 $km^2$ of forest.

Remarkable ring structures occur on the Galilean satellites of Jupiter, Callisto, and Ganymede. The largest is the 4000-km feature Valhalla on Callisto (Fig. 9), which consists of a bright central area up to 800 km in diameter, surrounded by a darker terrain with bright ridges 20–30 km apart. This zone is about 300 km wide and gives way to an outer zone with **graben** or rift-like features 50–100 km apart. These (very) multiring basins are generally considered to be of impact origin, but with the actual impact crater confined to the central area. The exterior rings are believed to be formed as a result of the original crater puncturing the outer, strong shell, or lithosphere, of these bodies. This permitted the weaker, underlying layer, the asthenosphere, to flow toward the crater, setting up stresses that led to fracturing and the formation of circumscribing scarps and graben.

On Callisto and Ganymede, there is also a unique class of impact craters that no longer have an obvious crater form but appear as bright, or high-albedo, spots on the surfaces of these bodies. These are known as palimpsests and are believed to have begun as complex craters but have had their topography relaxed by the slow, viscous creep of the target's icy crust over time. Palimpsests are old impact features and may have been formed when the icy satellites were young and relatively warm, with a thin crust possibly incapable of retaining significant topography.

Other anomalous crater forms are developed on Ganymede and Callisto. On these icy satellites, most craters larger than 25 km have a central pit or central dome (Fig. 10), rather than a central peak. Pit and dome craters are shallower than other craters of comparable size, and

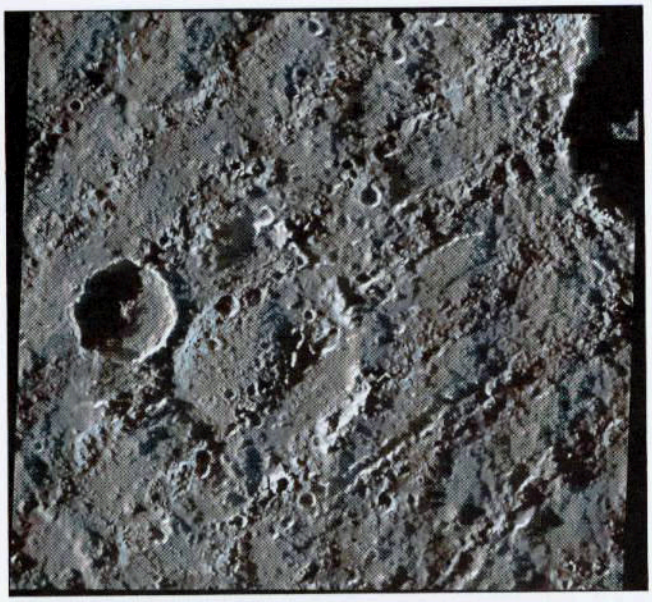

**FIGURE 10** Complex crater Har, 50 km in diameter, on Callisto, with a central dome in place of a central peak. The origin of the central mound is some form of response to the weak icy nature of the target material. A smaller (20 km) and younger central peak complex crater with a central peak, Tindr, occurs on the western rim of Har (*Galileo*).

it has been suggested that the pits are due to the formation of slushy or fluid material by impact melting and the domes are due to uplift of the centers of the craters as a result of layers in the crust with different mechanical properties. The fact that some craters on these icy bodies are anomalous has been ascribed to a velocity effect, as higher impact velocities result in greater melting of the target, or to changes in the mechanical behavior of the crust and its response to impact with time. Interpretations of the origin of the various anomalous crater forms on the icy satellites, however, are generally not well constrained.

## 1.2 Crater Dimensions

The depth–diameter relations for craters on the terrestrial or silicate planets are given in Table 1. (Relations are in the form $d = aD^b$, where $d$ is apparent depth, $D$ is rim-crest diameter, and units are in kilometers.). Other relations involving parameters such as rim height, rim width, central peak diameter, and central peak height can be found in the literature. Due to the abundant detailed imagery and low rate of crater-modifying process, such as erosion, the best-defined morphometric relations for fresh impact craters are from the Moon.

Simple craters have similar apparent depth–diameter relationships on all the terrestrial planets (Table 1). At first glance, terrestrial craters appear to be shallower than their planetary counterparts. Compared to the other terrestrial planets, erosion is most severe on Earth, and crater rims are rapidly affected by erosion. Few terrestrial craters have well-preserved rims, and it is common to measure terrestrial crater depths with respect to the ground surface, which is known and is assumed to erode more slowly. In the case of other planetary bodies, depths are measured most often by the shadow that the rim casts on the crater floor. That is, the topographic measure is a relative one between the rim crest and the floor. Thus, the measurements of depth for Earth and for other planetary bodies are not exactly the same. For the very few cases in which the rim is well preserved

**TABLE 1** Apparent Depth-Diameter Relations for Craters on the Terrestrial Planets

| Planetary Body | Exponent (b) | Coefficient (a) | Gravity ($cm^{-2}$) |
|---|---|---|---|
| **Simple Craters** | | | |
| Moon | 1.010 | 0.196 | 162 |
| Mars | 1.019 | 0.204 | 372 |
| Mercury | 0.995 | 0.199 | 378 |
| Earth | 1.06 | 0.13 | 981 |
| **Complex Central Peak Craters** | | | |
| Moon | 0.301 | 1.044 | 162 |
| Mars | 0.25 | 0.53 | 372 |
| Mercury | 0.415 | 0.492 | 378 |
| Venus | 0.30 | 0.40 | 891 |
| Earth | | | |
| Sedimentary | 0.12 | 0.30 | 981 |
| Crystalline | 0.15 | 0.43 | 981 |

in terrestrial craters, depths from the top of the rim to the crater floor are comparable to those of similar-sized simple craters on the other terrestrial planets.

Unlike simple craters, the depths of complex craters with respect to their diameters do vary between the terrestrial planets (Table 1). While the sense of variation is that increasing planetary gravity shallows final crater depths, this is not a strict relationship. For example, martian complex craters are shallower than equivalent-sized mercurian craters (Table 1), even though the surface gravities of the two planets are very similar. This is probably a function of differences between target materials, with the trapped volatiles and relatively abundant sedimentary deposits making Mars' surface, in general, a weaker target. Mars has also evidence of wind and water processes, which will reduce crater-related topography by erosion and sedimentary infilling. The secondary effect of target strength is also well illustrated by the observation that terrestrial complex craters in sedimentary targets are shallower than those in crystalline targets (Table 1).

Data from the Galileo mission indicates that depth–diameter relationships for craters on the icy satellites Callisto, Europa, and Ganymede have the same general trends as those on the rocky terrestrial planets. Interestingly, the depth–diameter relationship for simple craters is equivalent to that on the terrestrial planets. Although the surface gravities of these icy satellites is only 13–14% of that of the Earth, the transition diameter to complex crater forms occurs at ~3 km, similar to that on the Earth. This may be a reflection of the extreme differences in material properties between icy and rocky worlds. There are also inflections and changes in the slopes of the depth–diameter relationships for the complex craters, with a progressive reduction in absolute depth at diameters larger than the inflection diameter. These anomalous characteristics of the depth–diameter relationship have been attributed to changes in the physical behavior of the crust with depth and the presence of subsurface oceans. [*See* EUROPA; GANYMEDE AND CALLISTO.]

## 2. Impact Processes

The extremely brief timescales and extremely high energies, velocities, pressures, and temperatures that accompany impact are not encountered, as a group, in other geologic processes and make studying impact processes inherently difficult. Small-scale impacts can be produced in the laboratory by firing projectiles at high velocity (generally below about 8 km $s^{-1}$) at various targets. Some insights can also be gained from observations of high-energy, including nuclear explosions. Most recently, "hydrocode" numerical models have been used to simulate impact crater formation. The planetary impact record also provides constraints on the process. The terrestrial record is an important source of ground-truth data, especially with regard to the subsurface nature and spatial relations at impact craters, and the effects of impact on rocks.

When an interplanetary body impacts a planetary surface, it transfers about half of its kinetic energy to the target. The kinetic energy of such interplanetary bodies is extremely high, with the mean impact velocity on the terrestrial planets for asteroidal bodies ranging from ~12 km $s^{-1}$ for Mars to over ~25 km $s^{-1}$ for Mercury. The impact velocity of comets is even higher. Long-period comets (those with orbital periods greater than 200 years) have an average impact velocity with Earth of ~55 km $s^{-1}$, whereas short-period comets have a somewhat lower average impact velocity. [*See* COMETARY DYNAMICS.]

### 2.1 Crater Formation

On impact, a shock wave propagates back into the impacting body and also into the target. The latter shock wave compresses and heats the target, while accelerating the target material (Fig. 11). The direction of this acceleration is perpendicular to the shock front, which is roughly hemispherical, so material is accelerated downward and outward. Because a state of stress cannot be maintained at a free surface, such as the original ground surface or the edges and rear of the impacting body, a series of secondary release or "rarefaction" waves are generated, which bring the shock-compressed materials back to ambient pressure. As the rarefaction wave interacts with the target material, it alters the direction of the material set in motion by the shock wave, changing some of the outward and downward motions in the relatively near-surface materials to outward and upward, leading to the ejection of material and the growth of a cavity. Directly below the impacting body, however, the two wave fronts are more nearly parallel, and material is still driven downward (Fig. 11).

These motions define the **cratering flow-field** and a cavity grows by a combination of upward ejection and downward displacement of target materials. This "transient cavity" reaches its maximum depth before its maximum radial dimensions, but it is usually depicted in illustrations at its maximum growth in all directions (Fig. 11). At this point, it is parabolic in cross section and, at least for the terrestrial case, has a depth-to-diameter ratio of about 1 to 3. As simple craters throughout the solar system appear to have similar depth–diameter ratios, the 1:3 ratio for the transient cavity can probably be treated as universal.

An asteroidal body of density 3 g $cm^{-3}$ impacting crystalline target rocks at 25 km $s^{-1}$ will generate initial shock velocities in the target faster than 20 km $s^{-1}$, with corresponding velocities over 10 km $s^{-1}$ for the materials set in motion by the shock wave. The rarefaction wave has an initial velocity similar to that of the shock wave but, because the target materials are compressed by the shock, the rarefaction has a smaller distance to cover to overtake

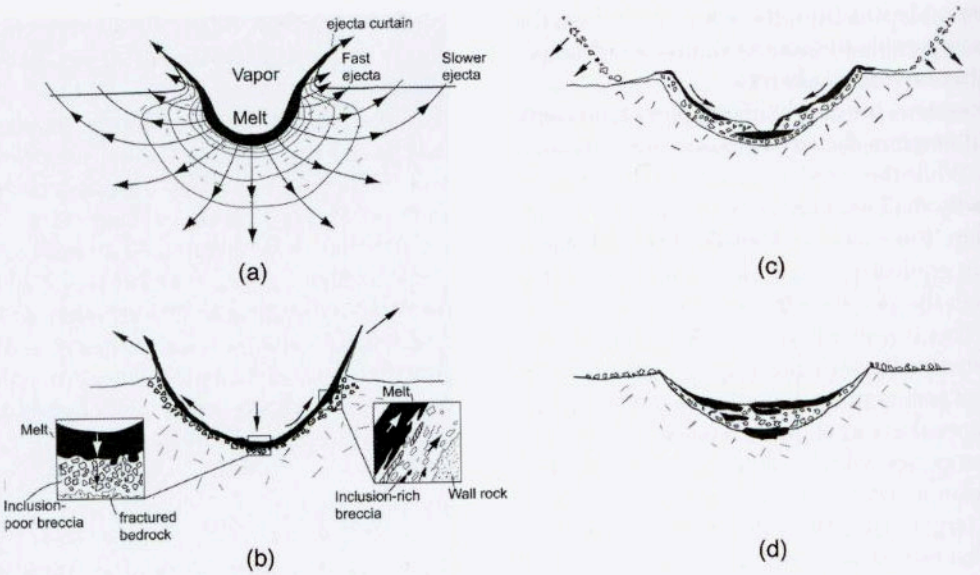


**FIGURE 11** Schematic illustration of the formation of a simple crater (Figs. 1 and 2). (a) On impact, the shock wave, indicated by the roughly hemispherical solid lines of shock pressure, propagates into the target rocks. Closer to the point of impact, the combination of the motions imparted by the shock and rarefaction waves has opened up a growing cavity through excavation and displacement of the target rocks. Melted and vaporized material is driven down into this expanding transient cavity. Ultimately, target rocks set in motion by the cratering flow-field will follow the paths outlined by the solid lines with arrows. (b) Close to the end of formation of the transient cavity formed by the cratering flow-field, with melted and shocked target rocks that are moving up the walls on their way to being ejected. (c) The unstable transient cavity walls collapse downward and inward, carrying the lining of melt and shocked target rocks into the cavity and mix them together with the wall rocks to form a breccia deposit. The collapse of the cavity walls also enlarges slightly the diameter of the final crater. (d) Final form of a simple crater with an interior breccia lens. (After Melosh, 1989.)

the moving material and alter its direction of movement. Transient-cavity growth is an extremely rapid event. For example, the formation of a 2.5 km diameter transient cavity will take only about 10 seconds on Earth.

The cratering process is sometimes divided into stages: initial contact and compression, excavation, and modification. In reality, however, it is a continuum with different volumes of the target undergoing different stages of the cratering process at the same time (Fig. 11). As the excavation stage draws to a close, the direction of movement of target material changes from outward to inward, as the unstable transient cavity collapses to a final topographic form more in equilibrium with gravity. This is the modification stage, with collapse ranging from landslides on the cavity walls of the smallest simple craters to complete collapse and modification of the transient cavity, involving the uplift of the center and collapse of the rim area to form central peaks and terraced, structural rims in larger complex craters.

The interior breccia lens of a typical simple crater is the result of this collapse. As the cratering flow comes to an end, the fractured and over-steepened cavity walls become unstable and collapse inward, carrying with them a lining of shocked and melted debris (Fig. 11). The inward-collapsing walls undergo more fracturing and mixing, eventually coming to rest as the bowl-shaped breccia lens of mixed unshocked and shocked target materials that partially fill simple craters (Fig. 11). The collapse of the walls increases the rim diameter, such that the final crater diameter is about 20% larger than that of the transient cavity. This is offset by the shallowing of the cavity accompanying production of the breccia lens, with the final apparent crater being about half the depth of the original transient cavity (Fig. 11). The collapse process is rapid and probably takes place on timescales comparable to those of transient-cavity formation.

Much of our understanding of complex-crater formation comes from observations at terrestrial craters, where it has been possible to trace the movement of beds to show that central peaks are the result of the uplift of rocks from depth (Fig. 4). Shocked target rocks, analogous to those found in the floors of terrestrial simple craters, constitute the central peak at the centers of complex structures, with the central structure representing the uplifted floor of the original transient cavity. The amount of uplift determined from terrestrial data corresponds to a value of approximately one tenth of the final rim-crest diameter. Further observations at terrestrial complex craters indicate excavation is also limited

to the central area and that the transient cavity diameter was about 50–65% of the diameter of the final crater. Radially beyond this, original near-surface units are preserved in the down-dropped annular floor. The rim area is a series of fault terraces, progressively stepping down to the floor (Fig. 3).

Although models for the formation of complex craters are less constrained than those of simple craters, there is a general consensus that, in their initial stages, complex craters were not unlike simple craters. At complex craters, however, the downward displacements in the transient cavity floor observed in simple craters are not locked in and the cavity floor rebounds upward (Fig. 12). As the maximum depth of the transient cavity is reached before the cavity's maximum diameter, it is likely that this rebound and reversal of the flow-field in the center of a complex crater occurs while the diameter of the transient cavity is still growing by excavation (Fig. 12). With the upward movement of material in the transient cavity's floor, the entire rim area of the transient cavity collapses downward and inward (Fig. 12), greatly enlarging the crater's diameter compared to that of the transient cavity. There have been a number of reconstructions of large lunar craters, in which the terraces are restored to their original, pre-impact positions, resulting in estimated transient cavity diameters of about 60% of the final rim-crest diameter. It is clear that

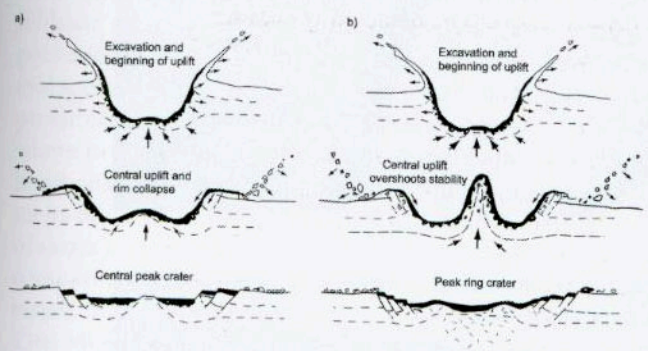


**FIGURE 12** Schematic illustration of the formation of complex crater forms: (a) central peak crater (Figs. 3 and 4) and (b) peak ring basin (Fig. 5). Initial excavation and displacement by the cratering flow-field are similar to that of a simple crater (Fig. 11). The downward displacement of the target rocks is permanent, but not locked in, and the floor of the transient cavity is uplifted, even as the transient cavity diameter continues to grow in diameter. As the floor rises, the rim of the transient cavity collapses downward and inward to create a final rim that is a structural set of faulted terraces, considerably enlarging the final rim diameter. Excavation of target material is limited to the central area, and the extensive modification of the transient cavity leads to a final crater with a flat floor and topographically uplifted target material in the center. In the case of the peak ring basin (b), the uplifted material is in excess of what can be accommodated in a central peak and it collapses to form a peak ring. (After Melosh, 1989.)

uplift and collapse, during the modification stage at complex craters, is extremely rapid and that the target materials behave as if they were very weak. A number of mechanisms, including "thermal softening" and "acoustic fluidization," by which strong vibrations cause the rock debris to behave as a fluid, have been suggested as mechanisms to produce the required weakening of the target materials.

There is less of a consensus on the formation of rings within impact basins. The most popular hypothesis for central peak basins is that the rings represent uplifted material in excess of what can be accommodated in a central peak (Fig.12). This may explain the occurrence of both peaks and rings in central peak basins but offers little explanation for the absence of peaks and the occurrence of only rings in peak ring and multiring basins. A number of analogies have been drawn with the formation of "craters" in liquids and semiconsolidated materials such as muds, where the initial uplifted peak of material has no strength and collapses completely, sometimes oscillating up and down several times. At some time in the formation of ringed basins, however, the target rocks must regain their strength, so as to preserve the interior rings. An alternative explanation is that the uplift process proceeds, as in central peak craters, but the uplifted material in the very center is essentially fluid due to impact melting. In large impact events, the depth of impact melting may reach and even exceed the depth of the transient cavity floor. When the transient cavity is uplifted in such events, the central, melted part has no strength and, therefore, cannot form a positive topographic feature, such as a central peak. Only rings from the unmelted portion of the uplifted transient cavity floor can form some distance out from the center (Fig. 5).

## 2.2 Changes in the Target Rocks

The target rocks are initially highly compressed by the passage of the shock wave, transformed into high-density phases, and then rapidly decompressed by the rarefaction wave. As a result, they do not recover fully to their preshock state but are of slightly lower density, with the nature of their constituent minerals changed. The collective term for these shock-induced changes in minerals and rocks is **shock metamorphism**. Shock metamorphic effects are found naturally in many lunar samples and meteorites and at terrestrial impact craters. They have also been produced in nuclear explosions and in the laboratory, through shock-recovery experiments. No other geologic process is capable of producing the extremely high transient pressures and temperatures required for shock metamorphism, and it is diagnostic of impact.

Metamorphism of rocks normally occurs in planetary bodies as a consequence of thermal and tectonic events originating within the planet. The maximum pressures and temperatures recorded in surface rocks by such metamorphic events in planetary crusts are generally on the order of

1 GPa (10 kb) and 1000°C. During shock metamorphism, materials deform along their "Hugoniot curves," which describe the locus of pressure–volume states achieved by the material while under shock compression. Shock metamorphic effects do not appear until the material has exceeded its "**Hugoniot elastic limit** (HEL)," which is on the order of 5–10 GPa for most geologic materials. This is the pressure–volume point beyond which the shocked material no longer deforms elastically and permanent changes are recorded on recovery from shock compression.

The peak pressures generated on impact control the upper limit of shock metamorphism. These vary with the type of impacting body and target material but are principally a function of impact velocity, reaching into the hundreds to thousands of GPa. For example, the peak pressure generated when a stony asteroidal body impacts crystalline rock at 15 km $s^{-1}$ is over 300 GPa, not much less than the pressure at the center of the Earth (~390 GPa). Shock metamorphism is also characterized by strain rates that are orders of magnitude higher than those produced by internal geologic processes. For example, the duration of regional metamorphism associated with tectonism on Earth is generally considered to be in the millions of years. In contrast, the peak strains associated with the formation of a crater 20 km in diameter are attained in less than a second.

### 2.2.1 SOLID EFFECTS

At pressures below the HEL, minerals and rocks respond to shock with brittle deformation, which is manifested as fracturing, shattering, and brecciation. Such features are generally not readily distinguished from those produced by endogenic geologic processes, such as tectonism. There is, however, a unique, brittle, shock-metamorphic effect, which results in the development of unusual, striated, and horse-tailed conical fractures, known as shatter cones (Fig. 13). Shatter cones are best developed at relatively low shock pressures (5–10 GPa) and in fine-grained, structurally homogeneous rocks, such as carbonates, quartzites, and basalts.

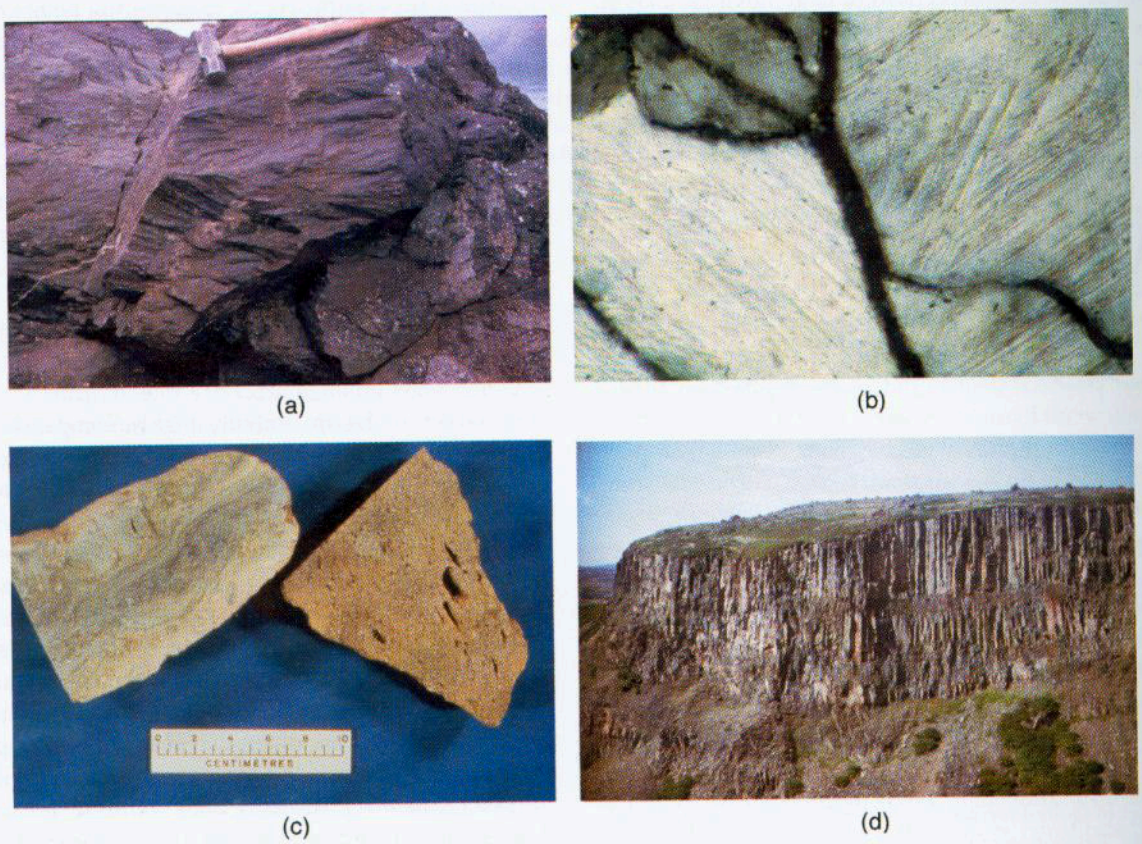


**FIGURE 13** Some shock metamorphic effects at terrestrial impact craters. (a) Shatter cones in basalt at the Slate Islands structure, Canada. (b) Photomicrograph of planar deformation features (e.g., in the left grain, thin parallel lines tending upwards to the right) in quartz from the Mistastin structure, Canada. Width of field of view is 0.5 mm, crossed polars. (c) Hand samples of target rocks from the Wanapitei structure, Canada, that are beginning to melt to form mixed mineral glasses and to vesiculate or froth. (d) Outcrop of coherent impact melt rock 80 m high, with columnar cooling joints, at the Mistastin structure, Canada.

Apart from shatter cones, all other diagnostic shock effects are microscopic in character. The most obvious are **planar deformation features** and **diaplectic glasses**. Planar deformation features are intensely deformed, are a few micrometers wide, and are arranged in parallel sets (Fig. 13). They are best known from the common silicate minerals, quartz and feldspar, for which shock-recovery experiments has calibrated the onset shock pressures for particular crystal orientations. They develop initially at ~10 GPa and continue to 20–30 GPa. The increasing effects of shock pressure are mirrored by changes in X-ray characteristics, indicative of the increasing breakdown of the internal crystal structure of individual minerals to smaller and smaller domains.

By shock pressures of ~30–40 GPa, quartz and feldspar are converted to diaplectic (from the Greek, "to strike") glass. These are solid-state glasses, with no evidence of flow, that exhibit the same outline as the original crystal. For this reason, they are sometimes referred to as thetamorphic (from the Greek, "same shape") glasses. The variety produced from plagioclase is known as maskelynite and was originally discovered in the Shergotty meteorite in 1872. The thermodynamics of shock processes are highly irreversible, so the pressure–volume work that is done during shock compression is not fully recovered upon decompression. This residual work is manifested as waste heat and, as a result, shock pressures of 40–50 GPa are sufficient to initiate melting in some minerals (Fig. 13). For example, feldspar grains show incipient melting and flow at shock pressures of ~45 GPa. Melting tends initially to be mineral specific, favoring mineral phases with the highest compressibilities and to be concentrated at grain boundaries, where pressures and temperatures are enhanced by reverberations of the shock wave. As a result, highly localized melts of mixed mineral compositions can arise. The effects of shock reverberations on melting are most obvious when comparing the pressures required to melt particulate materials, such as those that make up the lunar regolith [*see* THE MOON], and solid rock of similar composition. Shock recovery experiments indicate that intergranular melts can occur at pressures as low as 30 GPa in particulate basaltic material, compared to 45 GPa necessary to melt solid basalt.

Most minerals undergo transitions to dense, high-pressure phases during shock compression. Little is known, however, about the mineralogy of the high-pressure phases, as they generally revert to their low-pressure forms during decompression. Nevertheless, metastable high-pressure phases are sometime preserved, as either high-pressure **polymorphs** of preexisting low-pressure phases or high-pressure assemblages due to mineral breakdown. Some known high-pressure phases, such as diamond from carbon or stishovite from quartz ($SiO_2$), form during shock compression. Others, such as coesite ($SiO_2$), form by reversion of such minerals during pressure release. Several high-pressure phases that have been noted in shocked meteorites, however, are relatively rare at terrestrial craters. This may be due to post-shock thermal effects, which are sufficiently prolonged at a large impact crater to inhibit preservation of metastable phases.

### 2.2.2 MELTING

The waste heat trapped in shocked rocks is sufficient to result in whole-rock melting above shock pressures of ~60 GPa. Thus, relatively close to the impact point, a volume of the target rocks is melted and can even be vaporized (Figs. 11 and 12). Ultimately, these liquids cool to form impact melt rocks. These occur as glassy bodies in ejecta and breccias, as dikes in the crater floor, as pools and lenses within the breccia lenses of simple craters (Figs. 2 and 11), and as annular sheets surrounding the central structures and lining the floors of complex craters and basins (Figs. 4, 12, and 13). Some terrestrial impact melt rocks were initially misidentified as having a volcanic origin. In general, however, impact melt rocks are compositionally distinct from volcanic rocks. They have compositions determined by a mixture of the compositions of the target rocks, in contrast to volcanic rocks that have compositions determined by internal partial melting of more mafic and refractory progenitors within the planetary body's mantle or crust.

Impact melt rocks can also contain shocked and unshocked fragments of rocks and minerals. During the cratering event, as the melt is driven down into the expanding transient cavity (Figs. 11 and 12), it overtakes and incorporates less-shocked materials such as clasts, ranging in size from small grains to large blocks. Impact melt rocks that cool quickly generally contain large fractions of clasts, while those that cool more slowly show evidence of melting and resorption of the clastic debris, which is possible because impact melts are initially a superheated mixture of liquid melt and vapor. This is another characteristic that sets impact melt rocks apart from volcanic rocks, which are generally erupted at their melting temperature and no higher.

## 3. Impacts and Planetary Evolution

As the impact flux has varied through geologic time, so has the potential for impact to act as an evolutionary agent. The ancient highland crust of the Moon records almost the complete record of cratering since its formation. Crater counts combined with isotopic ages on returned lunar samples have established an estimate of the cratering rate on the Moon and its variation with time. Terrestrial data have been used to extend knowledge of the cratering rate, at least in the Earth–Moon system, to more recent geologic time. The lunar data are generally interpreted as indicating an exponential decrease in the rate until ~4.0 billion years (Ga) ago, a slower decline for an additional billion years, and a relatively constant rate, within a factor of two, since ~3.0 Ga

ago. The actual rate before ~4.0 Ga ago is imprecisely known, as there is the question of whether the ancient lunar highlands reflect all of the craters that were produced (i.e., a production population) or only those that have not been obliterated by subsequent impacts (i.e., an equilibrium population). Thus, it is possible that the oldest lunar surfaces give only a minimum estimate of the ancient cratering rate. Similarly, there is some question as to whether the largest recorded events, represented by the major multiring basins on the Moon, occurred over the relatively short time period of 4.2–3.8 Ga ago (the "called lunar cataclysm") or were spread more evenly with time. [*See* THE MOON.]

### 3.1 Impact Origin of Earth's Moon

The impacts of the greatest magnitude dominate the cumulative effects of the much more abundant smaller impacts in terms of affecting planetary evolution. In the case of Earth, this would be the massive impact that likely produced the Moon. Earth is unique among the terrestrial planets in having a large satellite and the origin of the Moon has always presented a problem. The suggestion that the Moon formed from a massive impact with Earth was originally proposed some 30 years ago, but, with the development of complex numerical calculations and more efficient computers, it has been possible more recently to model such an event. Most models involve the oblique impact of a Mars-sized object with the proto-Earth, which produces an Earth-orbiting disk of impact-produced vapor, consisting mostly of mantle material from Earth and the impacting body. This disk, depleted in volatiles and enriched in refractory elements, would cool, condense, and accrete to form the Moon. [*See* THE MOON.] In the computer simulations, very little material from the iron core of the impacting body goes into the accretionary disk, accounting for the low iron and, ultimately, the small core of the Moon. In addition to the formation of the Moon, the effects of such a massive impact on the earliest Earth itself would have been extremely severe, leading to massive remelting of Earth and loss of any existing atmosphere.

### 3.2 Early Crustal Evolution

Following planetary formation, the subsequent high rate of bombardment by the remaining "tail" of accretionary debris is recorded on the Moon and the other terrestrial planets and the icy satellites of the outer solar system that have preserved some portion of their earliest crust. Due to the age of its early crust, the relatively large number of space missions, and the availability of samples, the Moon is the source of most interpretations of the effects of such an early, high flux. In the case of the Moon, a minimum of 6000 craters with diameters greater than 20 km are believed to have been formed during this early period. In addition, ~45 impacts produced basins, ranging in diameter from Bailly at 300 km, through the South Pole–Aitken Basin at 2600 km, to the putative Procellarum Basin at 3500 km, the existence of which is still debated. The results of the *Apollo* missions demonstrate clearly the dominance of impact in the nature of the samples from the lunar highlands. Over 90% of the returned samples from the highlands are impact rock units, with 30–50% of the hand-sized samples being impact melt rocks. The dominance of impact as a process for change is also reflected in the age of the lunar highland samples. The bulk of the near-surface rocks, which are impact products, are in the range of 3.8–4.0 Ga old. Only a few pristine, igneous rocks from the early lunar crust, with ages >3.9 Ga, occur in the *Apollo* collection. Computer simulations indicate that the cumulative thickness of materials ejected from major craters in the lunar highlands is 2–10 km. Beneath this, the crust is believed to be brecciated and fractured by impacts to a depth of 20–25 km.

The large multiring basins define the major topographic features of the Moon. For example, the topography associated with the Orientale Basin (Fig. 6), the youngest multiring basin at ~3.8 Ga and, therefore, the basin with the least topographic relaxation, is over 8 km, somewhat less than Mt. Everest at ~9 km. The impact energies released in the formation of impact basins in the 1000 km size range are on the order of $10^{27}$–$10^{28}$ J, one to ten million times the present annual output of internal energy of Earth. The volume of crust melted in a basin-forming event of this size is on the order of a $1 \times 10^6$ km$^3$. Although the majority of crater ejecta is generally confined to within ~2.5 diameters of the source crater, this still represents essentially hemispheric redistribution of materials in the case of an Orientale-sized impact on the Moon.

Following formation, these impact basins localized subsequent endogenic geologic activity in the form of tectonism and volcanism. A consequence of such a large impact is the uplift of originally deep-seated isotherms and the subsequent tectonic evolution of the basin, and its immediate environs is then a function of the gradual loss of this thermal anomaly, which could take as long as a billion years to dissipate completely. Cooling leads to stresses, crustal fracturing, and basin subsidence. In addition to thermal subsidence, the basins may be loaded by later mare volcanism, leading to further subsidence and stress.

All the terrestrial planets experienced the formation of large impact basins early in their histories. Neither Earth nor Venus, however, retains any record of this massive bombardment, so the cumulative effect of such a bombardment on the Earth is unknown. Basin-sized impacts will have also affected any existing atmosphere, hydrosphere, and potential biosphere. For example, the impact on the early Earth of a body in the 500 km size range, similar to the present day asteroids Pallas and Vesta, would be sufficient to evaporate the world's present oceans, if only 25% of the impact energy were used in vaporizing the water. Such an event would have effectively sterilized the surface of Earth. The planet would have been enveloped by an atmosphere of hot rock and water vapor that would radiate heat downward

onto the surface, with an effective temperature of a few thousand degrees. It would take thousands of years for the water-saturated atmosphere to rain out and reform the oceans. Models of impact's potential to frustrate early development of life on Earth indicate that life could have survived in a deep marine setting at 4.2–4.0 Ga, but smaller impacts would continue to make the surface inhospitable until ~4.0–3.8 Ga.

### 3.3 Biosphere Evolution

Evidence from the Earth–Moon system suggests that the cratering rate had essentially stabilized to something approaching a constant value by 3.0 Ga. Although major basin-forming impacts were no longer occurring, there were still occasional impacts resulting in craters in the size range of a few hundred kilometers. The terrestrial record contains remnants of the Sudbury, Canada, and Vredefort, South Africa, structures, which have estimated original crater diameters of ~250 km and ~300 km, respectively, and ages of ~2 Ga. Events of this size are unlikely to have caused significant long-term changes in the solid geosphere, but they likely affected the biosphere of Earth. In addition to these actual Precambrian impact craters, a number of anomalous spherule beds with ages ranging from ~2.0 to 3.5 Ga. have been discovered relatively recently in Australia and South Africa. Geochemical and physical evidence (shocked quartz) indicate an impact origin for some of these beds; at present, however, their source craters are unknown. If, as indicated, one of these spherule beds in Australia is temporally correlated to one in South Africa, its spatial extent would be in excess of 32,000 $km^2$.

At present, the only case of a direct physical and chemical link between a large impact event and changes in the biostratigraphic record is at the "Cretaceous–Tertiary boundary," which occurred ~65 million years (Ma) ago. The worldwide physical evidence for impact includes: shock-produced, microscopic planar deformation features in quartz and other minerals; the occurrence of stishovite (a high-pressure polymorph of quartz) and impact diamonds; high-temperature minerals believed to be vapor condensates; and various, generally altered, impact-melt spherules. The chemical evidence consists primarily of a geochemical anomaly, indicative of an admixture of meteoritic material. In undisturbed North American sections, which were laid down in swamps and pools on land, the boundary consists of two units: a lower one, linked to ballistic ejecta, and an upper one, linked to atmospheric dispersal in the impact fireball and subsequent fallout over a period of time. This fireball layer occurs worldwide, but the ejecta horizon is known only in North America.

The Cretaceous–Tertiary boundary marks a mass extinction in the biostratigraphic record of the Earth. Originally, it was thought that dust in the atmosphere from the impact led to global darkening, the cessation of photosynthesis, and cooling. Other potential killing mechanisms have been suggested. Soot, for example, has also been identified in boundary deposits, and its origin has been ascribed to globally dispersed wildfires. Soot in the atmosphere may have enhanced or even overwhelmed the effects produced by global dust clouds. Recently, increasing emphasis has been placed on understanding the effects of vaporized and melted ejecta on the atmosphere. Models of the thermal radiation produced by the ballistic reentry of ejecta condensed from the vapor and melt plume of the impact indicate the occurrence of a thermal-radiation pulse on Earth's surface. The pattern of survival of land animals 65 Ma ago is in general agreement with the concept that this intense thermal pulse was the first global blow to the biosphere.

Although the record in the Cretaceous–Tertiary boundary deposits is consistent with the occurrence of a major impact, it is clear that many of the details of the potential killing mechanism(s) and the associated mass extinction are not fully known. The "killer crater" has been identified as the ~180 km diameter structure, known as Chicxulub, buried under ~1 km of sediments on the Yucatan peninsula, Mexico. Variations in the concentration and size of shocked quartz grains and the thickness of the boundary deposits, particularly the ejecta layer, point toward a source crater in Central America. Shocked minerals have been found in deposits both interior and exterior to the structure, as have impact melt rocks, with an isotopic age of 65 Ma.

Chicxulub may hold the clue to potential extinction mechanisms. The target rocks include beds of anhydrite ($CaSO_4$), and model calculations for the Chicxulub impact indicate that the $SO_2$ released would have sent anywhere between 30 billion and 300 billion tons of sulfuric acid into the atmosphere, depending on the exact impact conditions. Studies have shown that the lowering of temperatures following large volcanic eruptions is mainly due to sulfuric-acid aerosols. Models, using both the upper and lower estimates of the mass of sulfuric acid created by the Chicxulub impact, lead to a calculated drop in global temperature of several degrees Celsius. The sulfuric acid would eventually return to Earth as acid rain, which would cause the acidification of the upper ocean and potentially lead to marine extinctions. In addition, impact heating of nitrogen and oxygen in the atmosphere would produce $NO_x$ gases that would affect the ozone layer and, thus, the amount of ultraviolet radiation reaching the Earth's surface. Like the sulfur-bearing aerosols, these gases would react with water in the atmosphere to form nitric acid, which would result in additional acid rains.

The frequency of Chicxulub-size events on Earth is on the order of one every ~100 Ma. Smaller, but still significant, impacts occur on shorter timescales and could affect the terrestrial climate and biosphere to varying degrees. Some model calculations suggest that dust injected into the atmosphere from the formation of impact craters as small as 20 km could produce global light reductions and temperature disruptions. Such impacts occur on Earth with a frequency of approximately two or three every million years

but are not likely to have a serious affect upon the biosphere. The most fragile component of the present environment, however, is human civilization, which is highly dependent on an organized and technologically complex infrastructure for its survival. Though we seldom think of civilization in terms of millions of years, there is little doubt that if civilization lasts long enough, it could suffer severely or even be destroyed by an impact event.

Impacts can occur on historical timescales. For example, the Tunguska event in Russia in 1908 was due to the atmospheric explosion of a relatively small body at an altitude of ~10 km. The energy released, based on that required to produce the observed seismic disturbances, has been estimated as being equivalent to the explosion of ~10 megatons of TNT. Although the air blast resulted in the devastation of ~2000 $km^2$ of Siberian forest, there was no loss of human life. Events such as Tunguska occur on timescales of a thousand of years. Fortunately, 70% of the Earth's surface is ocean and most of the land surface is not densely populated.

## 4. Planetary Impactors

Apart from inferences from the compositions of asteroids, comets, and meteorites, the specific identification of actual impacting bodies is limited to occasional evidence from samples in or near craters on the Earth and Moon. For the majority of the ~170 impact craters so far identified on the Earth, however, the impactor types are either unknown or the identification is uncertain. The case for the Moon is no better. There are two methods used to determine projectile types: the physical identification of impactor fragments associated with a crater and identification of geochemical traces of an impactor component within impact melt rocks.

### 4.1 Physical Identification of Impactors

Although there is a widespread belief that the impactor is completely vaporized in large-scale impacts, this is not supported by numerical modeling. For example, at impact angles of ~45° or lower and velocities of 20 km $s^{-1}$, less than 50% of the impactor's mass vaporizes and the remaining fraction "survives" the impact, as melt or solid, and is deposited within or down range of the crater. Unfortunately, impactor fragments are rarely found associated with terrestrial impact craters. Any exposed remnants of the impactor are strongly affected by weathering processes and are normally destroyed after a few thousand years. As a result, virtually all impactor fragments have been found in the vicinity of very young terrestrial impact craters. Due to the size–frequency relation for impacts, these craters are also relatively small (<1.5 km) and were produced by iron meteorites, as this is the only type of small body that can survive atmospheric passage relatively intact and impact with enough remaining kinetic energy to create a crater.

Nevertheless, under conditions of rapid protection from weathering processes, it may be possible to find other types of impactor remnants associated with larger and older impact structures. This may be the case for a carbonaceous chondrite discovered at the Cretaceous–Tertiary boundary in a sedimentary core from the Pacific Ocean and inferred to be a small fragment of the impactor responsible for the Chicxulub structure. There are two other terrestrial cases where the physical presence of impactor-derived fragments has been inferred in larger impacts: East Clearwater, Canada ($D$ = 22 km) and Morokweng, South Africa ($D$ = 70 km). In both cases, however, the possible impactor materials have been reprocessed by their residence in impact melt rocks. The melt rocks at these craters have the highest known chemical admixture of impactor material of all terrestrial impact melt rocks (see later). Perhaps surprisingly, although there is no appreciable weathering on the Moon, few impactor fragments have been reported from the *Apollo* collection of lunar samples, although on the basis of geochemistry the lunar regolith is believed to contain a few percent of meteoritic material.

### 4.2 Chemical Identification of Impactor

The detection of a geochemical component of meteoritic material that has been mixed into impact melt rocks is the more common methodology for the identification of impactor type. Such a component has been detected at a number of terrestrial impact craters, and, in some cases, the impactor type has been identified with some degree of confidence (Table 2). The amount of impactor material in the melt rocks is typically <1%. Exceptions are at Morokweng and East Clearwater, where 7–10% impactor material occurs. The proportion of impactor component that can be incorporated to impact melts depends on the impact conditions, with the highest potential contributions occurring at low velocities and steep impact angles. The geochemical characterization of the incorporated impactor component can be achieved by examining Os isotopes, Cr isotopes, or elemental ratios, mainly the platinum group elements (PGEs), Ni, and Cr.

#### 4.2.1 OS ISOTOPES

Due to the relative enrichment of Re over Os during the differentiation of the Earth's crust from the mantle and the radioactive decay of $^{187}Re$ to $^{187}Os$, the $^{187}Os/^{188}Os$ ratios in terrestrial crustal rocks are higher than in both the Earth's mantle and most extraterrestrial materials. Thus, Os isotope ratios can be used to identify meteoritic components in terrestrial impact melt rock units. Impactor admixtures of less than 0.05% can be detected in the case of an impact into a continental crustal target. It is, however, sometimes not possible to determine whether the noncrustal component is from the Earths' mantle or an extraterrestrial

**TABLE 2 Impactor Types at Impact Craters**

| Name | Location | Age (Ma) | D (km) | Impactor Type | Evidence |
|---|---|---|---|---|---|
| Henbury | Australia | <0.005 | 0.16 | Iron; type IIIA | M, S |
| Odessa | United States | <0.05 | 0.17 | Iron; type IA | M |
| Boxhole | Australia | 0.0300 ± 0.0005 | 0.17 | Iron; type IIIA | M |
| Macha | Russia | <0.007 | 0.30 | Iron | M, S |
| Aouelloul | Mauritania | 3.1 ± 0.3 | 0.39 | Iron | S, Os |
| Monturaqui | Chile | <1 | 0.46 | Iron; type IA? | M, S |
| Wolfe Creek | Australia | <0.3 | 0.88 | Ion; type IIIB | M, S |
| Barringer | United States | 0.049 ± 0.003 | 1.19 | Iron; type IA | M, S |
| New Quebec | Canada | 1.4 ± 0.1 | 3.4 | Ordinary chondrite; type L? | S |
| Brent | Canada | 450 ± 30 | 3.8 | Ordinary chondrite; type L or LL | S |
| Sääksjärvi | Finland | ~560 | 6.0 | Stony iron ? | S |
| Wanapitei | Canada | 37.2 ± 1.2 | 7.5 | Ordinary chondrite; type L | S |
| Bosumtwi | Ghana | 1.03 ± 0.02 | 11 | Noncarbonaceous chondrite | S, Os, Cr |
| Lappajärvi | Finland | 77.3 ± 0.4 | 23 | Noncarbonaceous chondrite | S, Cr |
| Rochechouart | France | 214 ± 8 | 23 | Stony iron | S, Cr, |
| Ries | Germany | 15 ± 1 | 24 | No contamination | S |
| Clearwater East | Canada | 290 ± 20 | 26 | Ordinary chondrite; type LL | S |
| Clearwater West | Canada | 290 ± 20 | 36 | No contamination | S |
| Saint Martin | Canada | 220 ± 32 | 40 | No contamination | S |
| Morokweng | South Africa | 145.0 ± 0.8 | 70 | Ordinary chondrite; type LL | M,S, Cr |
| Popigai | Russia | 35 ± 5 | 100 | Ordinary chondrite; type L | S, Cr |
| Manicouagan | Canada | 214 ± 1 | 100 | No contamination | S |
| Chicxulub§ | Mexico | 64.98 ± 0.05 | 170 | Carbonaceous chondrite | M ,S, Os, Cr |
| Serenitatis Basin Spherule beds | Moon | 3.9 Ga | 740 | Ordinary chondrite; type LL | S, Cr |
| Hamersley Basin | Australia | 2.49 Ga | No crater | Enstatite chondrite, type EL ? | S, Cr |
| Baberton | South Africa | 3.1—3.5 Ga | No crater | Carbonaceous chondrite | S, Cr |

§ = enrichment in ejecta layer.
S = siderophile elements (PGE, Ni, Au); Cr = chromium isotopes; Os = Os isotopes; M = projectile fragment

source, and the method cannot be used to identify the type of impactor because the variation of the Os isotope ratios between known meteorite types is too small to act as a discriminator.

### 4.2.2 CR ISOTOPES

Chromium-isotope ratios of extraterrestrial materials differ from those of the Earth and the Moon. It is possible to distinguish between three groups of meteorites on the basis of Cr isotopes: (a) carbonaceous chondrites, (b) enstatite chondrites, and (c) all other types. The relatively high amounts of Cr in terrestrial and lunar rocks, however, restrict the use of this method. The characterization of the impactor type generally needs several percent of contamination, which is not common in terrestrial craters. One exception is measurements on Cretaceous–Tertiary boundary sediments from Stevens Klint, Denmark, and Caravaca, Spain, which have 5–10% extraterrestrial component. These data support the suggestion that the Chicxulub impactor was a carbonaceous chondrite [*See* METEORITES.]

### 4.2.3 ELEMENTAL RATIOS

Parameters for impactor identification can be derived from ratios of highly siderophile elements (i.e., those associated with Fe), such as the PGEs, Ni, and Au, along with Cr, which is a lithophile element (i.e., associated with Si) element. Relative to most meteorites, these elements are depleted in terrestrial crustal rocks, except where there are concentrations of mafic and ultramafic rocks. It has been argued that the amount of target rock mafic to ultramafic components in the impact melt rocks must be estimated in order to obtain a precise impactor composition. The complete determination of this "indigenous correction" is difficult for most terrestrial craters and essentially impossible for lunar impact craters. It has been have demonstrated, however, that the "indigenous correction" is not required, provided the impactor elemental ratios are calculated by using a mixing

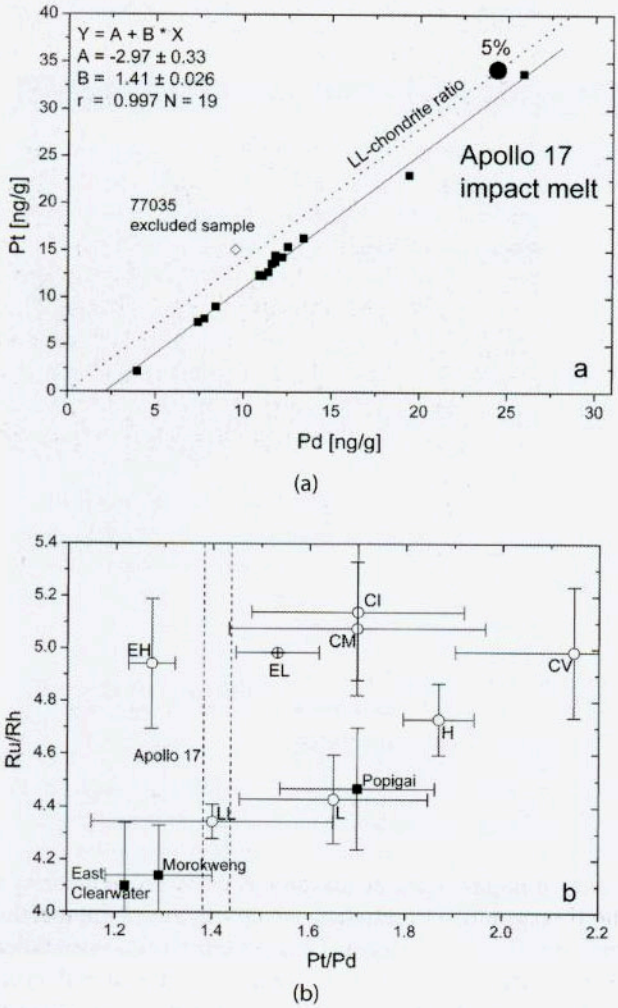


**FIGURE 14** Identification of impactor type. (a) Pt–Pd ratios and determination of impactor type in lunar impact melt rock from *Apollo 17*. Shown for comparison is the slope of equivalent elemental ratios in LL–chondrite meteorites and where an admixture of 5% of LL–chondrite would plot (black dot). (b) Comparison of elemental ratios relative to few impact craters with different classes of chondrites. Error bars on data points are 1 sigma error bars. The *Apollo 17* impact melt rock appears as vertical dashed lines, as Ru/Rh data are not available.

line, where the elemental ratios of the impactor can be calculated directly from the slope of the mixing line. This is illustrated in Fig. 14 for the melt rocks at Popigai (Russia), Morokweng (South Africa), East Clearwater (Canada), and *Apollo 17* impact melts (Serenitatis) from the Moon. There is essentially no effect of the composition of the target rocks on the slope of the mixing line, and the resulting projectile elemental ratios can be plotted together with the elemental ratios for the various classes of chondrites to provide a clear discrimination at the level of meteorite class (Fig. 14). It is, however, important to use elemental ratios that allow the best discrimination for a clear identification of the impactor type.

Within the various terrestrial impactor types identified to date, ordinary chondrites are by far the most common (Table 2). The reasons for the relative frequency of ordinary chondrite impactors for the Earth, and likely also the Moon, can be found in the Asteroid Belt. Ordinary chondrites are most likely related to S-class asteroids, which appear to be the most common asteroids in the main belt and among near-Earth asteroids (NEAs), although there is a possible observational bias due to their higher albedo compared to that of carbonaceous chondrites.

Although iron meteorites are responsible for all recent terrestrial craters smaller than 1.5 km in diameter, no unequivocal geochemical signature of iron impactors has yet been identified, at larger impact structures. Some terrestrial craters have no detectable extraterrestrial component in their impact rock units, and it has generally been assumed that the impactors were differentiated achondrites, which are relatively depleted in PGEs and Ni, and, thus, are very difficult to identify in terrestrial impact melt rocks. Differentiated asteroids are relatively rich in Cr and the use of Cr isotopes may be the only method to demonstrate that the impactor was an achondrite.

Although cometary impactors likely play a minor role (1–10% of the total population) in impacts in the Earth–Moon system, their identification is problematic. Their composition is essentially unknown with respect to their very small proportion of refractory elements, such as PGEs. [*See* PHYSICS AND CHEMISTRY OF COMETS.]

## Bibliography

French B. M. (1998). "Traces of Catastrophe: A Handbook of Shock-Metamorphic Effects in Terrestrial Meteorite Impact Structures," Lunar and Planetary Institute Contribution 954, Lunar and Planetary Institute, Houston.

Geological Society of America, Special Papers, 293 (1994), 339 (1999), 356 (2002), and 361 (2005).

Melosh, H. J. (1989). "Impact Cratering: A Geologic Process." Oxford Univ. Press, New York.

Spudis, P. D. (1993). "The Geology of Multi-ring Basins: The Moon and Other Planets." Cambridge Univ. Press, Cambridge, United Kingdom.